Contrasting effects of CO_2 fertilisation, land-use change and warming on seasonal amplitude of northern hemisphere CO_2 exchange

SUPPLEMENTARY MATERIAL

TABLE S1 – Trends in SCA_{NBP} estimated by each inversion and the LSM multi-model ensemble mean (simulation S3) for different periods in the two selected latitudinal bands. CarboScope provides several inversion estimates with an increasing number of assimilated sites. For consistency, trends in SCA_{NBP} are estimated in each of the periods covered by the CarboScope inversions (s76 for 1980-2015, s85 for 1985-2015, and s93 for 1993-2015). To determine whether the changes to the LSMs and forcings in TRENDYv6 could have contributed to improving their estimates of the SCA_{NBP} trends, we compared the results to the TRENDYv4 multi-model ensemble mean (for a group of 9 models) for 1982-2013. Values are provided in Tg C y^{-2} as in Figure 1, subscript and superscript values correspond to the 95% confidence interval limits of the trend fit and the asterisks indicate significant values (p<0.05). Because uncertainty in each dataset is calculated differently, we chose to present uncertainty in the trend only, but the footnotes indicate further details on uncertainty.

	$L_{>40N}$			$L_{25\text{-}40N}$		
Period	**CAMS[1]**	**CarboScope[2]**	**TRENDYv6[3]**	**CAMS[1]**	**CarboScope[2]**	**TRENDYv6[3]**
1980-2015	$17.3\ ^{21.8}_{12.9}$*	$13.3\ ^{16.6}_{10.1}$*(s76)	$9.5\ ^{12.8}_{6.1}$*	$-0.03\ ^{1.5}_{-2.1}$	$1.3\ ^{2.4}_{0.2}$*(s76)	$0.8^{1.9}_{-0.4}$
1985-2015	$16.2\ ^{21.9}_{10.6}$*	$11.7\ ^{16.7}_{6.7}$* (s85)	$10.6\ ^{15.1}_{6.2}$*	$-0.9\ ^{1.4}_{-3.1}$	$1.2\ ^{2.4}_{0.0}$*(s85)	$1.3\ ^{2.8}_{-0.2}$
1993-2015	$19.5\ ^{28.3}_{10.7}$*	$19.2\ ^{27.5}_{10.9}$* (s93)	$14.4\ ^{21.9}_{6.9}$*	$-1.3\ ^{2.4}_{-5.0}$	$4.6^{8.4}_{0.7}$*(s93)	$2.4^{4.8}_{0.0}$*
	$L_{>40N}$			$L_{25\text{-}40Nca}$		
Period	**CAMS**	**CarboScope**	**TRENDYv4[§]** **TRENDYv6[§]**	**CAMS**	**CarboScope**	**TRENDYv4[§]** **TRENDYv6[§]**
1982-2013	$14.6^{19.8}_{9.3}$*	$11.9^{15.7}_{8.2}$*(s76)	$6.7^{9.0}_{4.5}$* $9.6^{13.8}_{5.4}$*	$-1.3^{0.8}_{-3.4}$	$0.2\ ^{1.4}_{-1.0}$(s76)	$0.4^{1.3}_{-0.5}$ $0.8^{2.3}_{-0.6}$

[1] The uncertainty only represents the uncertainty of the linear fit due to year-to-year variability. Values do not include uncertainty in CAMS SCA. Errors in NBP fluxes have been calculated for each latitudinal band ($L_{>40N}$ and $L_{25\text{-}40N}$) as $1\sigma = \pm 0.1 PgC.yr^{-1}$. Errors in SCA_{NBP} should be smaller since some terms should cancel out.

[2] The uncertainty only represents the uncertainty of the linear fit due to year-to-year variability. An estimate of the additional uncertainty from the inversion calculation can be obtained by comparing trends estimated for different sensitivity runs around CarboScope s85_v4.1, shown in Figure S3.

[3] Values refer to the MMEM only. SCA trends and respective error-bars for individual models are shown in Figure S4.

[§]Values refer to the set of models used here that also contributed to TRENDYv4 (CLM4.5, ISAM, JSBACH, JULES, LPX, ORCHIDEE/ORCHIDEE-MICT) and VISIT).

Table S2 – Statistical models tested to evaluate the best predictors of trends in SCA_{NBP}. N/A indicates that no significant fit has been found for a given number of predictors.

		$L_{>40N}$			L_{25-40N}		
$N_{Predictors}$	**Dataset**	**Model**	**R^2_{adj}**	**AIC**	**Model**	**R^2_{adj}**	**AIC**
1	CAMS	$SCA_{NBP} \sim CO_2 + c$	0.63	-35.6	N/A	N/A	N/A
	CarboScope	$SCA_{NBP} \sim CO_2 + c$	0.65	-42.7	$SCA_{NBP} \sim CO_2 + c$	0.09	-6.6
	MMEM	$SCA_{NBP} \sim CO_2 + c$	0.48	-19.5	N/A	N/A	N/A
2	**CAMS**	**$SCA_{NBP} \sim T_{gs} + CO_2 + c$**	**0.74**	**-47.8**	$SCA_{NBP} \sim Fert + CO_2 + c$	0.01	7.7
	CarboScope	$SCA_{NBP} \sim T_{gs} + CO_2 + c$	0.69	-46.0	$SCA_{NBP} \sim T_{gs} + CO_2 + c$	0.45	-23.8
	MMEM	$SCA_{NBP} \sim T_{gs} + CO_2 + c$	0.53	-22.0	$SCA_{NBP} \sim T_{gs} + CO_2 + c$	0.17	-10.6
3	CAMS	N/A	N/A	N/A	**$SCA_{NBP} \sim Fert + T_{gs} + CO_2 + c$**	**0.08**	**6.0**
	CarboScope	$SCA_{NBP} \sim A_{Crop} + A_{For} + CO_2 + c$	0.67	-42.6	**$SCA_{NBP} \sim P_{gs} + T_{gs} + CO_2 + c$**	**0.49**	**-25.9**
	MMEM	**$SCA_{NBP} \sim A_{For} + T_{gs} + CO_2 + c$**	**0.57**	**-24.7**	**$SCA_{NBP} \sim WH + T_{gs} + CO_2 + c$**	**0.33**	**-17.1**
4	CAMS	N/A	N/A	N/A	$SCA_{NBP} \sim Fert + Irrig + T_{gs} + CO_2 + c$	0.05	6.0
	CarboScope	**$SCA_{NBP} \sim A_{Crop} + A_{For} + T_{gs} + CO_2 + c$**	**0.71**	**-46.8**	N/A	N/A	N/A
	MMEM	N/A	N/A	N/A	N/A	N/A	N/A

Table S3 – References for the AMERIFLUX datasets used in Figure S8. Full references provided in the Supplementary Material references.

Site	Ref	DOI
US-ARM	Sebastien Biraud (2002-)	http://dx.doi.org/10.17190/AMF/1246027
US-Bo1	Tilden Meyers (1996-)	http://dx.doi.org/10.17190/AMF/1246036
US-Br1	John Prueger, Tim Parkin (2001-)a	http://dx.doi.org/10.17190/AMF/1246038
US-Br3	John Prueger, Tim Parkin (2001-)b	http://dx.doi.org/10.17190/AMF/1246039
US-IB1	Roser Matamala (2005-)	http://dx.doi.org/10.17190/AMF/1246065
US-Ne1	Andy Suyker (2001-)a	http://dx.doi.org/10.17190/AMF/1246084
US-Ne2	Andy Suyker (2001-)b	http://dx.doi.org/10.17190/AMF/1246085
US-Ne3	Andy Suyker (2001-)c	http://dx.doi.org/10.17190/AMF/1246086
US-Ro2	John Baker, Tim Griffis (2003-2017)	http://dx.doi.org/10.17190/AMF/1418683
US-Twt	Dennis Baldocchi (2009-2017)	http://dx.doi.org/10.17190/AMF/1246140

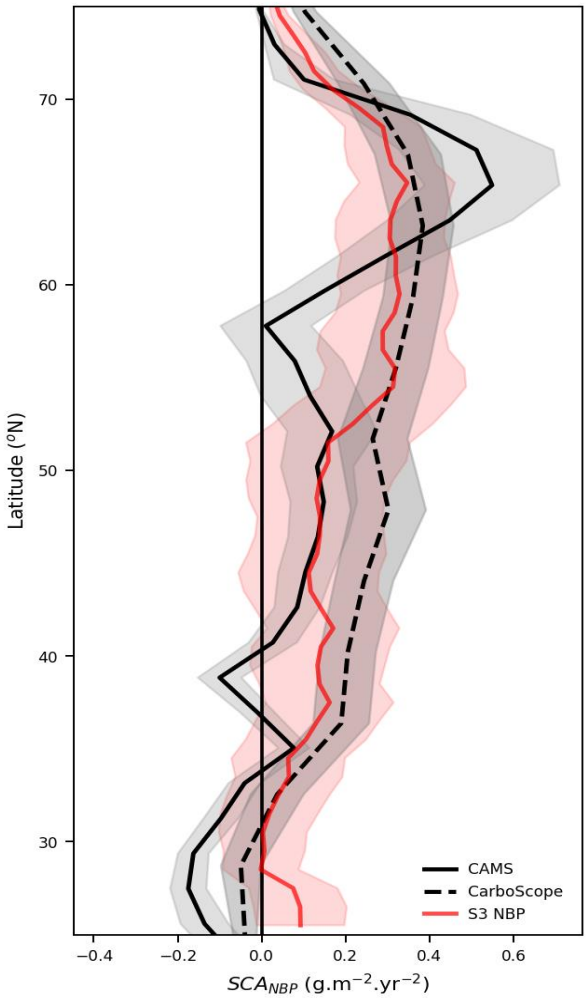

Figure S1 – Latitudinal distribution of SCA_{NBP} estimated by the two inversions and TRENDYv6 S3 (all forcings). The horizontal line separates the two latitudinal bands: $L_{>40N}$ covering latitudes >40°N (where both inversions estimate positive trends in SCA_{NBP}), and $L_{25\text{-}40N}$ covering the extra-tropical latitudes of the Northern Hemisphere (25-40°N). The shades indicate respectively the 95% confidence intervals for the trends in the case of inversions, and the model spread for LSMs.

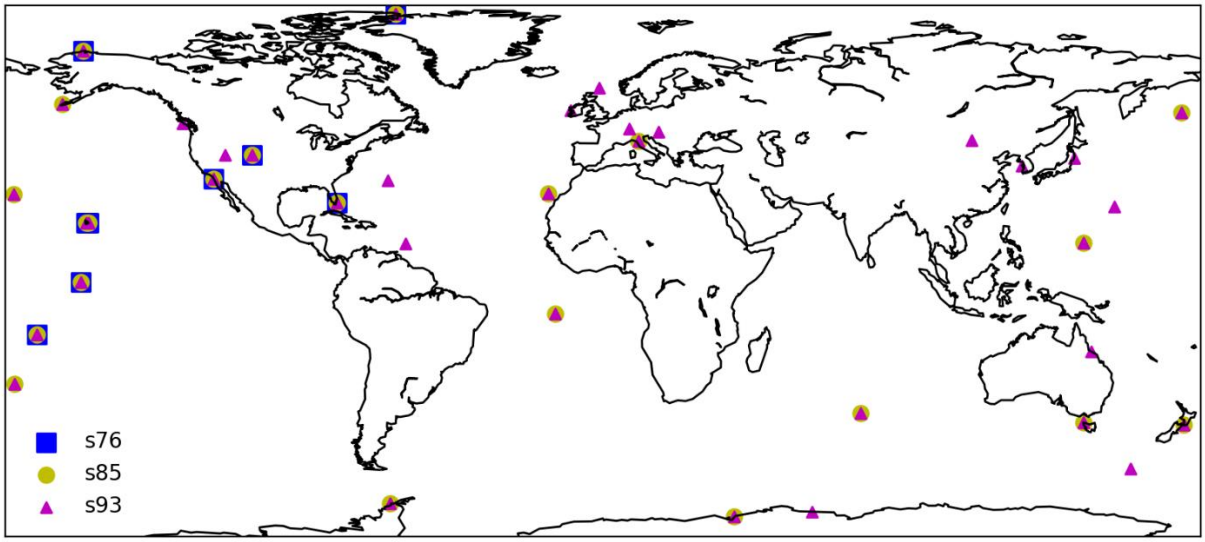

Figure S2 – Sites assimilated in the different versions of CarboScope v4.1 inversion: s76 (1976-2016), s85 (1985-2016) and s93 (1993-2016).

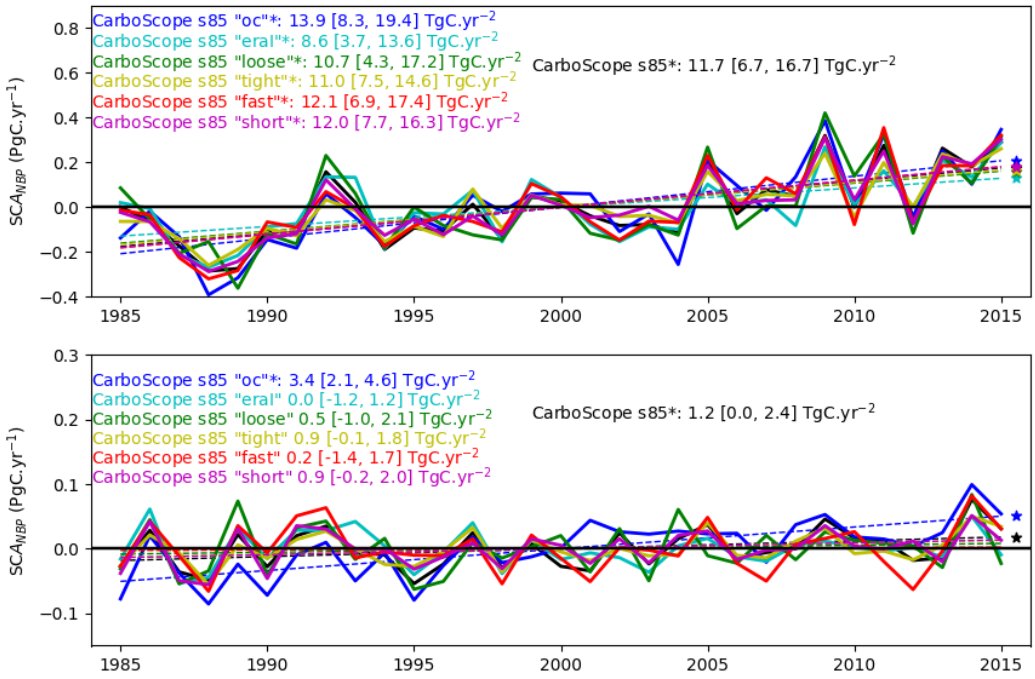

Figure S3 – Variability in SCA from different sensitivity tests around CarboScope s85, and respective trends. The different values provide an uncertainty range for s85_v4.1 results; this range should not differ much for the other versions (i.e. s76, s93, Table S1). The different tests performed consisted of *"oc"*: ocean fluxes fixed to pCO2-based estimates; *"eral"*: forcing the transport model with fields from ERA-Interim reanalysis instead of NCEP; *"loose"* and *"tight"*: scaling the a-priori sigma for all land and ocean flux components by 0.5 (dampening) and 2 (amplification), respectively; *"fast"*: reducing the length of a-priori temporal correlations by a factor 2; *"short"*: reducing the length of a-priori spatial correlations by a factor 3.

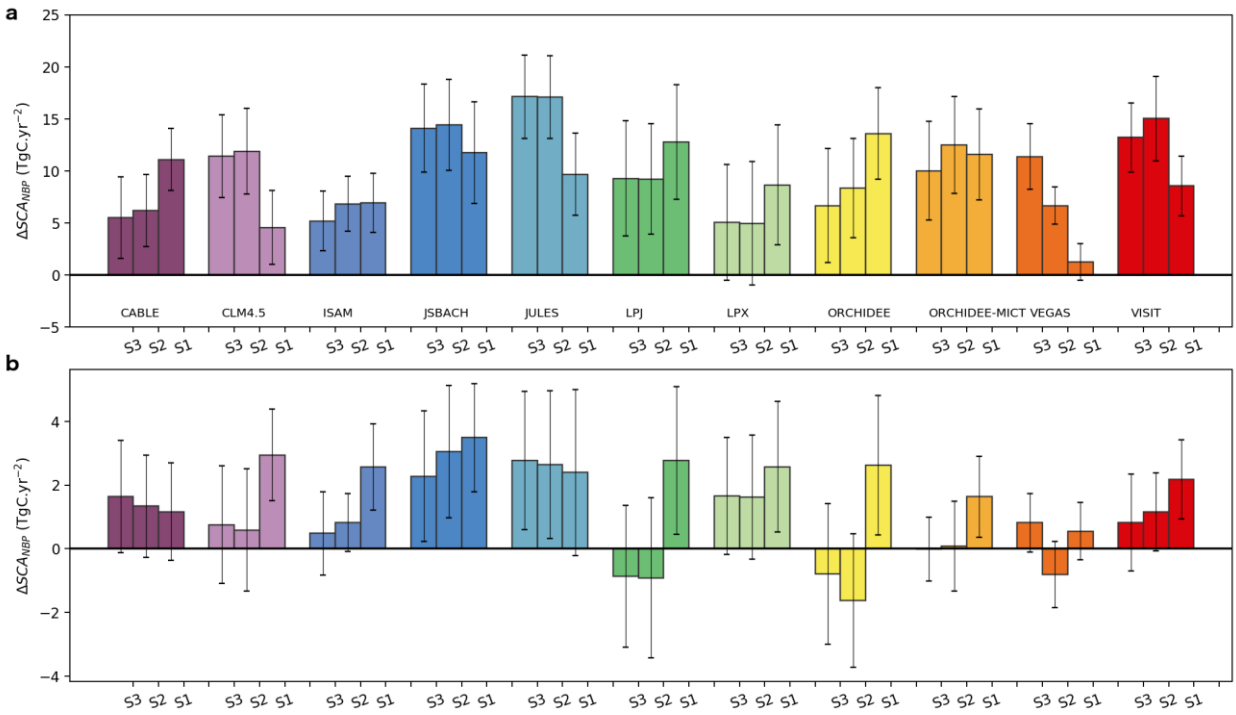

Figure S4 – Changes in SCA_{NBP} estimated by individual models for each of the TRENDYv6 experiments for the two latitudinal bands a) $L_{>40N}$ b) and $L_{25\text{-}40N}$). The error bars indicate the 95% confidence intervals for the trends. The labels in (a) indicate the corresponding model.

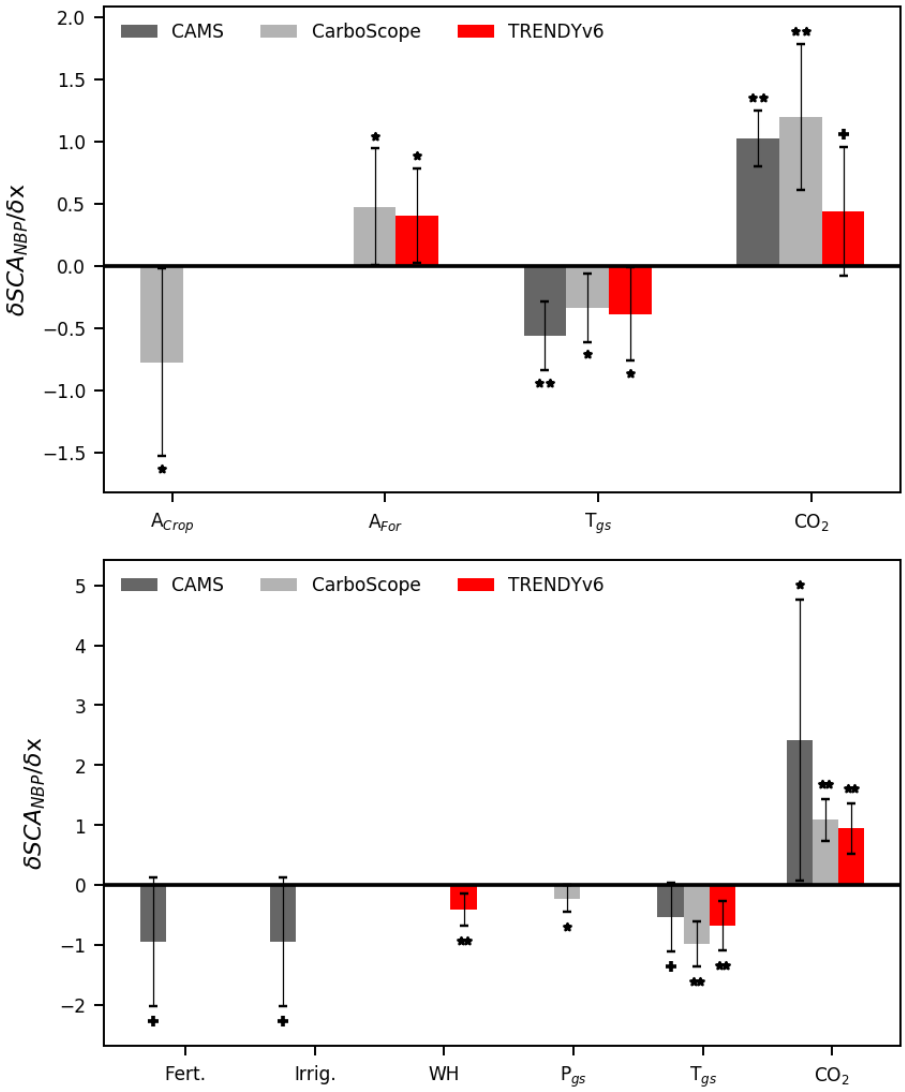

Figure S5 – Sensitivity of SCA_{NBP} to drivers for (a) $L_{>40N}$ and (b) $L_{25\text{-}40N}$. The coefficients of the GLM fit of SCA_{NBP} shown here were used in Figure 3 to calculate the contribution of each variable to the trends in SCA_{NBP}.

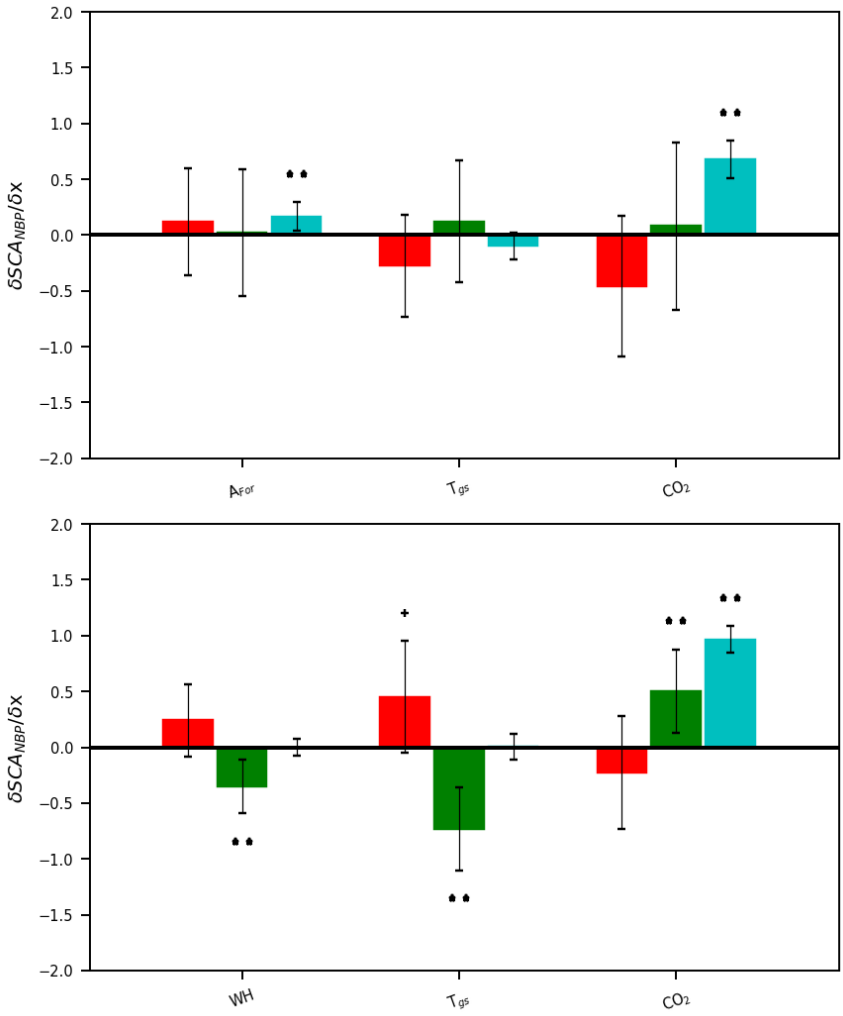

Figure S6 – Factorial verification of the drivers in TRENDY S3 for (a) >40°N and (b) 25-40°N. The MLRM fit to the partial fluxes for the effects of LULCC (S3-S2, red), climate (S2-S1, green), and CO_2 fertilisation (S1, cyan). Results should be compared to those in Figure S4. The significant predictors in the GLM fit to the LSMs in S3 should be detected in the corresponding factorial simulations. It should however be noted that management and fertilization are already included in S1 and S2 for some models. The difference between S3 and S2 (LULCC effects) mainly suggest LULCC processes and does not identify the effect of CO_2. The effect of CO_2 is identified mainly by the difference in S1-S0 and S2-S1, possibly due to synergies between CO_2 fertilisation and climate change. The effect of temperature should be evident in the difference between S2 and S1 (effects of climate), consistently found in $L_{25\text{-}40N}$.

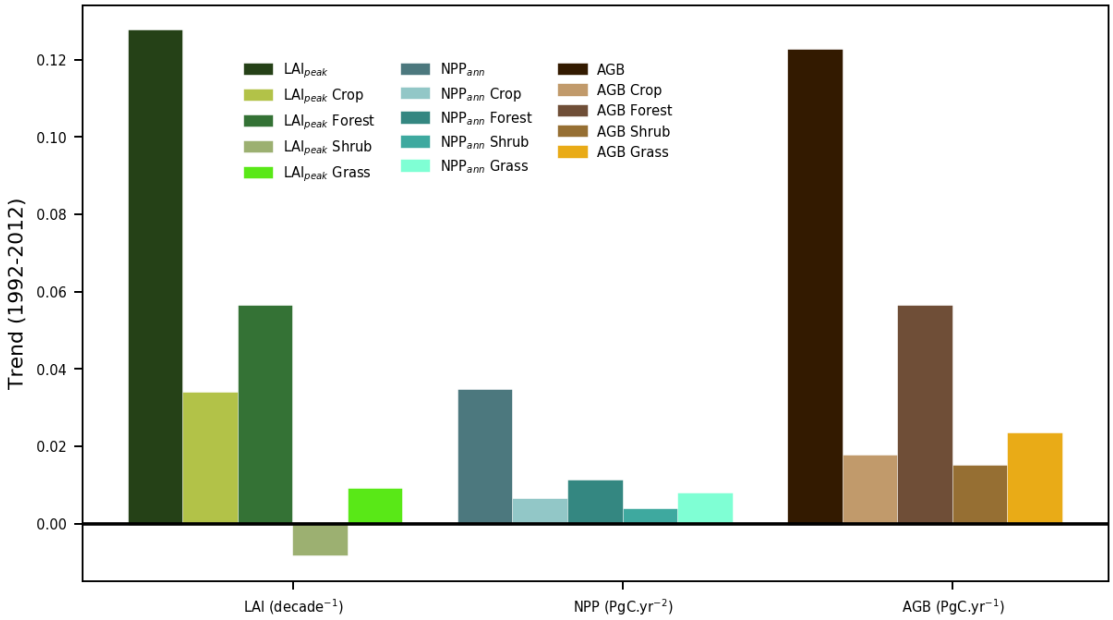

Figure S7 – Trends in vegetation growth for the land-cover types for 1992-2015. We analysed the trends in LAI (from GIMMS [Zhu et al., 2013]), NPP (based on AVHRR, from [Smith et al., 2016]), and AGB stocks (from passive-microwave satellite data for vegetation optical depth [Liu et al., 2016]). Trends in each variable were aggregated for the northern extra-tropical latitudes (>25°N, corresponding to $L_{>40N}$+ $L_{25\text{-}40N}$; left bar for each variable) and for four land-cover classes: cropland, forest, shrubland, and grassland. These classes were based on the ESA-CCI land-cover maps provided for 1992-2015, and each time interval was separately aggregated to account for changes in land-cover composition. The data sets covered distinct periods, so we selected periods of at least 20 years common to ESA-CCI LC and the vegetation data sets (1992-2012 for LAI, 1992-2011 for NPP, and 1993-2012 for AGB stocks).

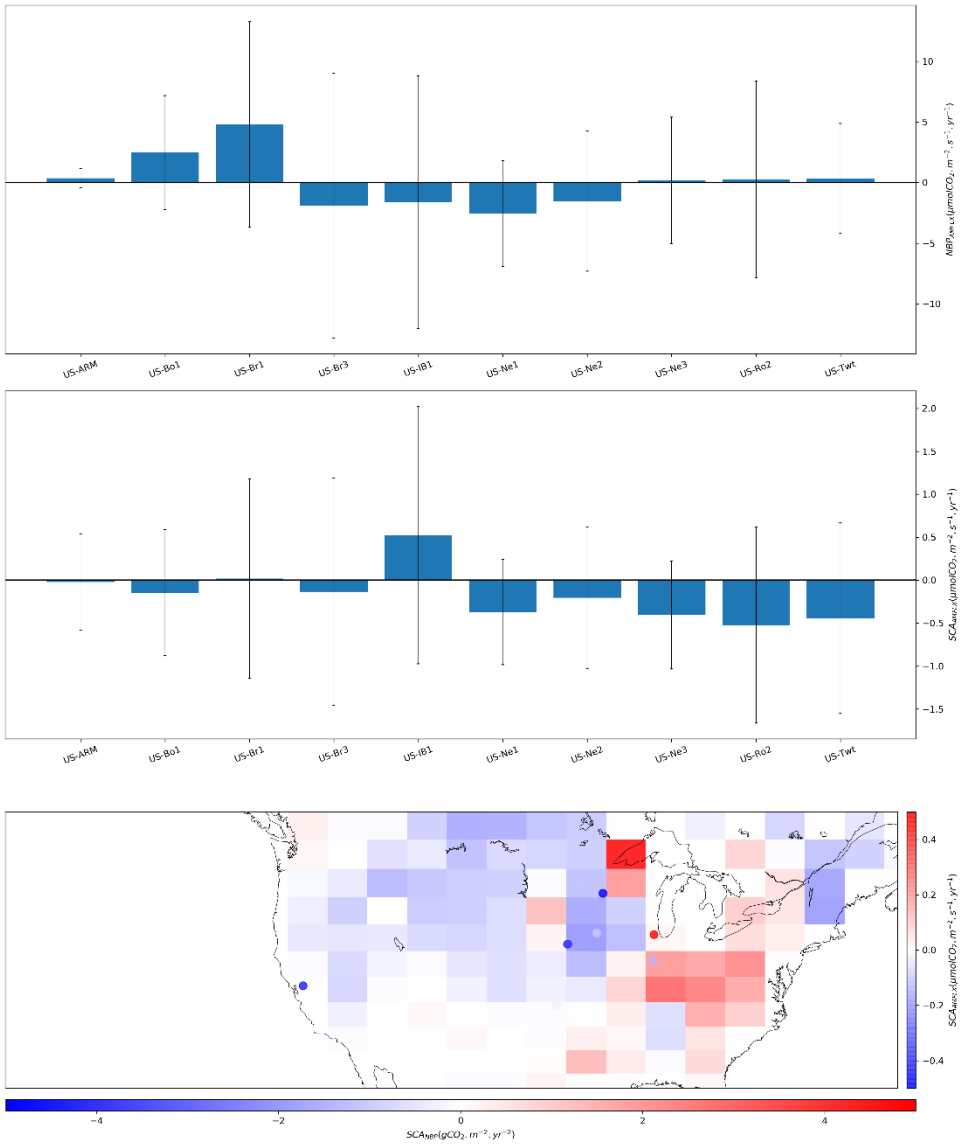

Figure S8 – Trends in the annual seasonal CO_2 exchange in (a) AMERIFLUX cropland sites where eddy covariance was measured, and (b) comparison with the spatial patterns of CAMS. The trends in seasonal net ecosystem exchange were calculated for all AMERIFLUX sites in the continental USA (https://ameriflux.lbl.gov/sites/site-search/#filter-type=all&igbp=CRO&region=USA,Table S3). Data are provided at 30-min intervals during the various periods. Only sites with data for at least 5 years were selected, and the data were first filtered to remove noise and outliers by fitting annual Fourier functions (with four harmonics) to individual years to obtain a smooth seasonal cycle. The amplitude of the seasonal exchange was then defined as the difference between the maximum and minimum net land-to-atmosphere flux. The bars indicate the trends estimated for the corresponding validity periods (variable), and the error bars indicate the 95% confidence intervals. None of the sites has a significant trend (the error bars cross the x-axis), although most tend to be negative. The spatial pattern of the trends was then compared to the CAMS map, and CAMS also reports negative trends over most of midwestern USA where most areas are intensely cropped, consistent with the sign of the trends in the AMERIFLUX data.

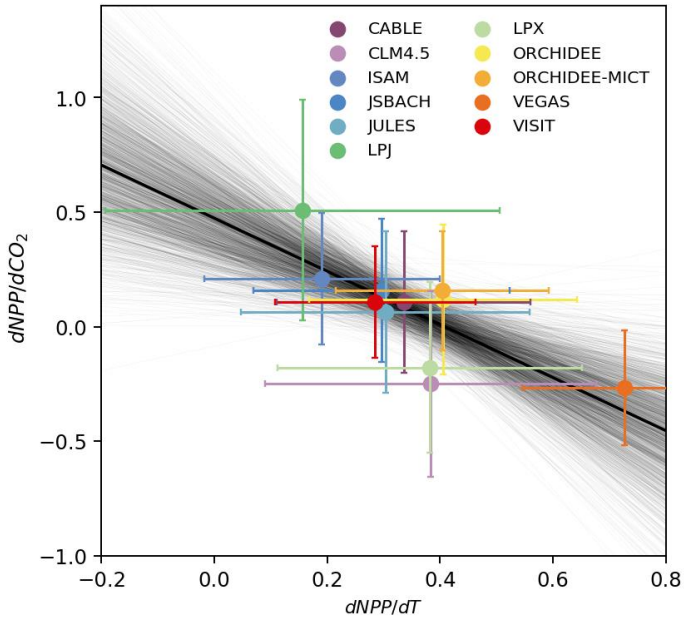

Figure S9 – Relationship between model sensitivity of net primary productivity (NPP) to CO2 (*y axis*) and to T (*x axis*). The distribution of the grey lines shows uncertainty in the relationship between the two variables.

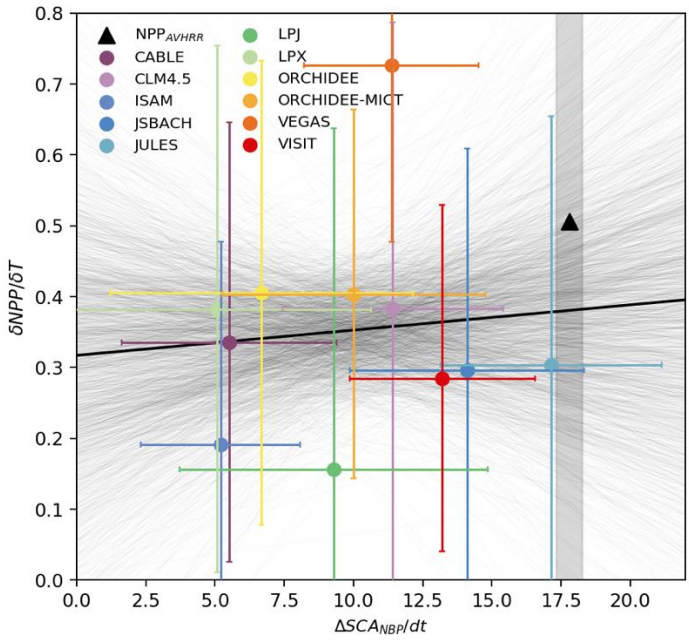

Figure S10 – Relationship between modelled trends in SCA_{NBP} and the sensitivity of (a) net primary productivity (NPP) to growing season temperature LSMs. The shaded areas indicate the inversion ranges for SCA_{NBP}. The distribution of the grey lines shows uncertainty in the relationship between the two variables.

Supplementary References

Sebastien Biraud (2002-) AmeriFlux US-ARM ARM Southern Great Plains site- Lamont, doi:10.17190/AMF/1246027.

Tilden Meyers (1996-) AmeriFlux US-Bo1 Bondville, doi: 10.17190/AMF/1246036

John Prueger, Tim Parkin (2001-)a AmeriFlux US-Br1 Brooks Field Site 10- Ames, doi: 10.17190/AMF/1246038

John Prueger, Tim Parkin (2001-)b AmeriFlux US-Br3 Brooks Field Site 11- Ames, doi: 10.17190/AMF/1246039

Roser Matamala (2005-) AmeriFlux US-IB1 Fermi National Accelerator Laboratory- Batavia (Agricultural site), doi: 10.17190/AMF/1246065

Andy Suyker (2001-)a AmeriFlux US-Ne1 Mead - irrigated continuous maize site, doi: 10.17190/AMF/1246084

Andy Suyker (2001-)b AmeriFlux US-Ne2 Mead - irrigated maize-soybean rotation site, doi: 10.17190/AMF/1246085

Andy Suyker (2001-)c AmeriFlux US-Ne3 Mead - rainfed maize-soybean rotation site, doi: 10.17190/AMF/1246086

John Baker, Tim Griffis (2003-2017) AmeriFlux US-Ro2 Rosemount- C7, doi: 10.17190/AMF/1418683

Dennis Baldocchi (2009-2017) AmeriFlux US-Twt Twitchell Island, doi: 10.17190/AMF/1246140